Desalination and Water Treatment
www.deswater.com

doi: 10.5004/dwt.2017.20546

71 (2017) 289–301
April

Dynamic simulation of spherical particle settling in quiescent water

Sivasamy Balasubramanian[a,*], Krishnan Suresh[a], Ramasamy Karthikeyan[b]

[a]*Department of Chemical Engineering, SRM University, Kattankulathur, Tamil Nadu – 603203, India, Tel. 91-9840754728; email: balasubramanian.s@ktr.srmuniv.ac.in (S. Balasubramanian), Tel. +91-9600094917; email: suresh.k@ktr.srmuniv.ac.in (K. Suresh)*
[b]*Retired Principal, Anjalai Ammal Mahalingam Engineering College, Kovil Venni, Thiruvarur District, Tamil Nadu – 614403, India, Tel. +91-9940561915; email: drrkarthi@yahoo.com*

Received 16 August 2016; Accepted 26 January 2017

ABSTRACT

An examination of the behaviour of free settling particles in Newtonian fluids is important in designing multiphase systems for widespread applications in industrial water treatment processes. Through transient three-dimensional simulations based on the arbitrary Lagrangian–Eulerian (ALE) moving mesh technique, the present study evaluates the behaviour of a rigid sphere settling or falling freely in water, a Newtonian fluid at rest under the influence of gravity. Simulations were carried out for sphere-to-fluid density ratios between 1.3 and 1.92; wall effect was reduced by setting up blockage ratio as 0.01 and corresponding moderate particle Reynolds numbers (Re_p) ranging from 131 to 1,097. This paper presents linear velocity, trajectory, transient drag coefficient, angular velocity and lift coefficient of a spherical particle settling freely in quiescent water. Data from the study was validated by comparing with published research literature results. Findings revealed that firstly, when a sphere descends from its initial position, its trajectory is defined by the onset of its rotation and lift force. Secondly, the effect of sphere rotation on transient drag coefficient is reported. It is also observed that for the entire range of Re_p studied, ALE is one of the powerful tools to capture accurate behaviour of solid–fluid interaction systems. However, it requires frequent re-meshing and fine mesh around the solid–fluid interface.

Keywords: Settling velocity; CFD simulation; Drag coefficient; Angular velocity; Lift coefficient

1. Introduction

It is extremely vital to understand the hydrodynamic forces acting on particles, as well as the trajectory or path taken by the particle when it moves relative to a fluid (Newtonian or non-Newtonian) in design and operation of industrial wastewater treatment processes systems where two-phase (fluid–solid) interaction is involved. Examples of such systems include clarifiers, gravity thickeners, sedimentation tanks and fluidized beds [1–9]. Secondly, an insight into sphere dynamics during its transportation in a fluid facilitates the determination of fluid–solid interphase momentum, heat and mass transfer rates, and particle residence time. The dynamics of a solid sphere settling through Newtonian fluid (water) at rest is complicated by factors such as size of the sphere, ratio of sphere-to-fluid density, fluid viscosity, descending velocity of sphere, particle Reynolds number (Re_p) and the drag coefficient (C_D). Although interest in the study of free fall of solid spheres in a quiescent fluid dates back to the era of Newton [10] and Stokes [11], it still continues to excite and evoke interest due to the complexity associated with (a) the degree of freedom in free fall and (b) structure of wake behind the sphere [12–15]. A comprehensive review of the extensive research work of numerous scientists on the terminal velocity of free-falling spheres in an unbounded Newtonian fluid has been presented by Hartman and Yates [16], till year 1999. In the past decades, steady-state

* Corresponding author.

behaviour of the spheres falling in stationary incompressible Newtonian fluid was tirelessly investigated by many authors and contributed wealth of knowledge. In contrast to steady-state motion of sphere, relatively very less work is reported for unsteady sphere fall in a Newtonian fluid at rest [17–19]. It is evident from research literature that the velocity of sphere fall in a fluid at rest is strongly a function of the drag force exerted by the fluid on the sphere particles.

The "drag force" is a resistive force experienced by solid particles while moving relative to unbounded quiescent fluid. Its magnitude is a function of particle size, velocity and fluid properties such as density and viscosity [5]. The drag force experienced by a sphere falling freely under gravity in a Newtonian fluid at rest is comparable with the drag force (standard drag) experienced by a sphere held fixed in fluid flow characterised by intermediate particle Reynolds numbers up to a certain level. It is also observed that validation of drag coefficient between freely falling and fixed spheres plays an important role in the design of chemical and biological reactors based on the principle of inverse fluidized beds [13,20]. Furthermore, in the experiments on the settling velocities of round and smooth spheres falling in calm water, Boillat and Graf [21] compared the drag coefficients of free-falling spheres with the standard drag coefficients and found that differences between the two were because of experimental limitations. They also emphasised the need for further research on the difference between the standard drag and free-falling sphere drag. Mordant and Pinton [22] observed that spherical particles falling freely under gravity in a quiescent fluid exhibited oscillatory behaviour at the initial stage of transition for intermediate Reynolds numbers; oscillation was later stabilised with time. This oscillatory behaviour of the sphere may be the reason behind the difference in drag coefficient that exists between the sphere held in uniform flow and the sphere falling freely in the fluid. In this regime, the sphere-to-fluid density ratio may be a governing factor, but the physics behind the oscillatory behaviour has not yet been clearly illustrated by analytical or numerical techniques. Niazmand and Renksizbulut [23] enumerated the dynamic forces acting on the fixed sphere rotating at constant speed in a fluid of uniform flow with particle Reynolds number up to 300 and dimensionless angular velocity of 1. They noted that an increase in angular velocity of the sphere increased the drag coefficient beyond Re_p of 50.

Yu et al. [24] performed dynamic simulations of spheres falling in a Newtonian fluid contained in a vertical tube based on the finite difference, distributed Lagrange multiplier (DLM) method and reported fall velocity, trajectory and angular velocity values of spheres for Re_p ranging from 20 to 400. Their results demonstrated that at low Re_p, the sphere approached the tube axis monotonically, whereas at high Re_p, the sphere followed a spiral trajectory closer to the tube wall than the tube axis; experimental studies conducted by Horowitz and Williamson [25], however, did not report similar findings. Jenny et al. [26] performed numerical simulations to investigate the transition scenario of an ascending/falling sphere in Newtonian fluid and discovered that the path of a falling sphere followed an oblique oscillating trajectory and became chaotic. The same authors also observed that at a high Re_p ~400, the wake shedding behind the sphere impacted the sphere motion thereby affecting the drag coefficient. Veldhuis and Biesheuvel [27] carried out similar experiments to visualise the trajectory and wake structure of falling spheres at intermediate Re_p (~250–1,970) by means of the stereoscopic Schlieren technique. The images obtained by them reiterated that falling spheres followed a path deviating from the straight vertical line (i.e., oblique and oscillating) because of an irregular wake structure formed behind the sphere wake.

The experimental work of Horowitz and Williamson [25] using particle image velocimetry for investigating freely rising and falling spheres in a quiescent fluid revealed a steady oblique path at Re_p 450 for a sphere-to-fluid density ratio of 1.4. However, it was difficult to record sphere rotation during particle movement due to experimental difficulties. Similar results were obtained by Veldhuis et al. [28]. Numerical simulations using a fictitious domain method were performed by Rupesh et al. [29] for a freely falling sphere in a fluid at rest. Their efforts unraveled the fact that the loss of axisymmetric wake behind the sphere at Re_p 210 resulted in rotation and lateral migration of the sphere and, in addition, a deviation in sphere drag when compared with the standard drag. The numerical results presented by Zhou and Dušek [30] show the complete transition scenario of sphere falling freely in fluid. However, it was stated that the helical trajectory with accurate periodicity might have the link with the vibrating state trajectories that was experimentally found by Horowitz and Williamson [14]. Furthermore, they also pointed out that this link was not elucidated fully, and this work was also sought the need of quantitative characterisation of chaotic state as future work.

In recent times, advanced numerical simulation techniques that are an improvement over earlier experimental methods provide a flexible alternative to evaluate multiphase flow problems. Several authors have investigated solid–fluid interactions using numerical simulations [29,31–33]. In particular, the flow behaviour of solid spheres in a quiescent Newtonian fluid evaluated by computational simulations has received much attention [24,26]. The simulation techniques employed include: (a) a fixed mesh technique namely DLM and (b) a moving mesh technique known as arbitrary Lagrangian–Eulerian (ALE) method. Of the two, ALE was found to be more advantageous, yielding relatively more accurate results because of mesh adaptivity [31,32].

The present study used ALE moving mesh simulation to study the behaviour of rigid sphere freely falling under gravity in water at rest. Continuity and momentum equations (governing equations for fluid flow) were coupled with equations pertaining to motion of a sphere. The ability to capture the complex behaviour of sphere motion in a quiescent fluid is numerically expensive, e.g., the quality of mesh around the sphere breaks down within a shorter time duration when the Re_p increases, thereby necessitating frequent re-meshing in the fluid domain in order to get a more accurate flow field around the rigid solid sphere.

From the above discussion of research literature on both experimental and numerical investigations, it follows that the data on time-averaged drag coefficients of spheres falling freely in water at rest are still largely unclear. Moreover, the observed time-averaged drag coefficients were significantly different from the standard drag because of non-vertical trajectories and rotation of sphere in quiescent Newtonian

fluid, especially at intermediate Reynolds numbers between 210 and 1,500. Furthermore, the underlying reason behind the deviation in time-averaged drag coefficient is not well addressed in the available research literature. Therefore, the present study focuses on the behaviour of rigid solid sphere falling freely under gravity in quiescent Newtonian fluid (water) at intermediate particle Reynolds numbers using computational fluid dynamics (CFD) simulations.

This research report is structured as follows: firstly, those definitions are presented that are associated with the free fall of a sphere in water at rest and that were used in this study. This is followed by a discussion of problem formulation and solution methodology for the phenomena. Next, validation of simulation results is provided by corroboration with data from published literature. Also discussed are details of the effect of sphere trajectory and angular velocity on transient drag coefficients for the intermediate Re_p. Finally, a discussion is presented pertaining to the lift force experienced by the spherical particle and also the sphere residence time.

2. Definitions used in the simulation studies

Given below are the definitions of various parameters that have been used in the simulation studies of the present research undertaking. It is necessary to be familiar with these terms in order to understand the phenomenon of sphere falling freely in quiescent fluid (water).

2.1. Density ratio

Density ratio (ρ_r), defined as the ratio of sphere density to water, is a measure of the driving force. For all the cases studied in the present investigation, a density ratio >1 was considered. The dimensionless form of density ratio is given by:

$$\rho_r = \frac{\rho_p}{\rho_f} \tag{1}$$

where ρ_p is the density of the particle, and ρ_f is the density of fluid.

2.2. Sphere displacement

Sphere displacement as it falls freely under gravity in *x*-, *y*- and *z*-direction is given in the dimensionless form, which is the ratio of sphere displacement to the sphere diameter as given below:

$$X = \frac{D_X}{D_p},\quad Y = \frac{D_Y}{D_p},\quad Z = \frac{D_Z}{D_p} \tag{2}$$

where D_x, D_y and D_z are displacement of sphere in *x*-, *y*- and *z*-direction.

2.3. Terminal velocity

A particle of size D_p falling through a fluid at rest under the action of gravity initially accelerates and then continues to attain a constant velocity until the acceleration of the particle becomes zero. The velocity at which the acceleration of particle becomes zero is called the "terminal velocity" $\langle U_t \rangle$ of the particle, also known as "time-averaged terminal velocity" of the particle.

2.4. Particle Reynolds number

For a sphere moving in a fluid, the particle Reynolds number (Re_p) is defined as the ratio of inertial forces to the fluid viscous forces. It is given as:

$$\mathrm{Re}_p = \frac{D_p \langle U_t \rangle \rho_f}{\mu_f} \tag{3}$$

where D_p is the sphere diameter, and $\langle U_t \rangle$ ρ_f and μ_f are the time-averaged velocity of sphere, density and viscosity of the fluid (water), respectively.

2.5. Local and time-averaged drag coefficient

Under steady-state conditions, a force balance between the fluid and solid yields a drag coefficient (C_D), which is given as:

$$C_D = \frac{4gD_p\Delta\rho}{3\rho_f U_t^2} \tag{4}$$

where $\Delta\rho$ is density difference between the fluid and sphere; *g* is acceleration due to gravity. In the present study, time-averaged drag coefficient $\langle C_D \rangle$ was calculated by considering the time-averaged sphere velocity $\langle U_t \rangle$ as given in the following equation:

$$\langle C_D \rangle = \frac{4gD_p\Delta\rho}{3\rho_f \langle U_t^2 \rangle} \tag{5}$$

2.6. Standard drag curve

The solid line (curve) shows the variation of drag coefficient with Re_p for a sphere fixed in flow of fluid. This solid line is termed "standard drag curve" and is used to correlate the behaviour of a sphere falling in a fluid at rest with that of a fixed sphere in a fluid flow. Although research literature provides many standard drag correlations [34], a well-known relationship proposed by Turton and Levenspiel [35] was used in this study to estimate the standard drag coefficient. It is given by the following expression:

$$C_D = \frac{24}{\mathrm{Re}_p}(1 + 0.173\,\mathrm{Re}_p^{0.657}) + \frac{0.413}{1 + 16300\,\mathrm{Re}_p^{-1.09}} \tag{6}$$

The above expression (Eq. (6)) is applicable for wide range of Reynolds numbers ($10^{-2} < Re_p < 2 \times 10^5$), which includes creeping, transition and turbulent regimes. The relation is based on the data obtained from fixed sphere in fluid flow and falling spheres [28].

2.7. Best number

N_D or the "Best number" as given in Clift et al. [34] can be used to determine the terminal velocity of a sphere falling in a fluid. The present investigation used the Best number to compare experimental data with simulation data obtained from results of the study. The relation used is given below:

$$N_D = \frac{4\rho_f \Delta\rho (2a)^3}{3\mu_f^{\ 2}} \tag{7}$$

where a is the radius of the sphere in mm.

2.8. Lift coefficient

Lift force can be quantified by the lift coefficient [36] as given below:

$$\langle C_L \rangle = \frac{F_L}{1/2\rho_f U_t^2 \pi / 4D_p^2} \tag{8}$$

where $\langle F_L \rangle$ is the lift force that acts on the sphere. In the present study, the lift force experienced by the sphere falling in water was obtained by integrating local pressure and viscous forces along the sphere surface in a moving direction:

$$\langle F_L \rangle = \left[\iint (P + \tau_W) \boldsymbol{n}\, ds \right] \cdot \boldsymbol{e}_y \tag{9}$$

where τ_W is the wall shear stress; $\boldsymbol{n}$ is the unit vector pointing outward from the surface of the sphere; and $\boldsymbol{e}_y$ is the unit vector in y coordinate, i.e., direction of sphere falling in the water.

2.9. Residence time of sphere

In the present study, the residence time of the sphere refers to the time that the sphere takes to cross a fixed distance when it descends (falls) from initial position in the Newtonian fluid domain.

3. Problem formulation

3.1. Computational domain

Consider a rigid sphere of diameter D_p placed at the top of a square-shaped duct filled with Newtonian fluid (water) with density ρ_f and viscosity μ_f as shown in the three-dimensional (3D) Fig. 1(a). The height of the duct being 0.7 m, the sphere was placed at 0.1 m distance away from the top of the duct. Initially the particle was at rest, and a distance of 0.4 m travelled by the sphere from the initial position was considered. The ratio of sphere diameter to breadth or width (blockage ratio) of the duct was maintained as 0.01 in order to reduce the wall effect. The spheres used in the study varied in diameter from 1.6 to 4.0 mm. The density ratio (solid-to-fluid) was maintained between 1.3 and 1.92 for all sphere diameters. The computational domain was generated with a 3D grid, non-uniform unstructured mesh using the commercial software ICEM CFX®V13. Finer mesh was created around the sphere surface to resolve the rapid changes that occur with velocities, while coarser mesh was created in the bulk of the fluid. The entire computational domain adopted in this study is presented in Figs. 1(a)–(c).

The governing equations (continuity and Navier Stokes – momentum) solved for the phenomena are listed below:

Continuity equation:

$$\nabla \cdot \boldsymbol{u} = 0 \quad \text{(for incompressible Newtonian fluid)} \tag{10}$$

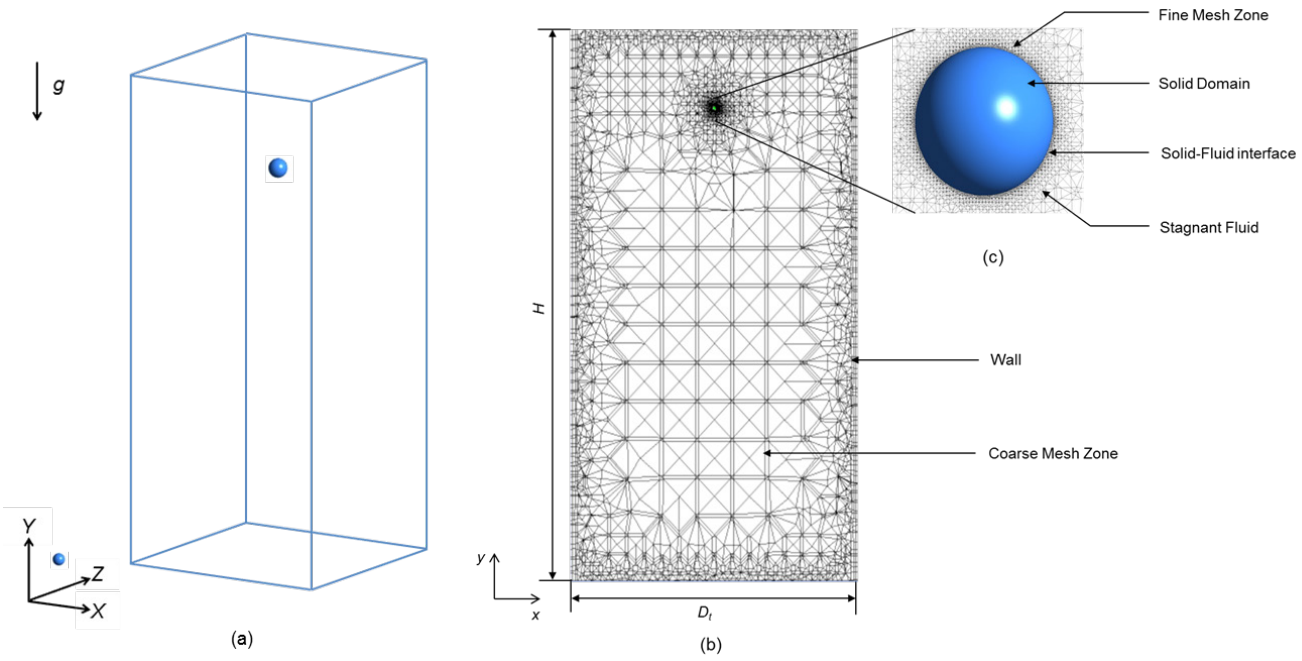

Fig. 1. (a) 3D Geometry considered for the simulation; (b) typical mesh created for the falling sphere placed at centre in a quiescent Newtonian fluid; and (c) magnified view of mesh near the sphere and fluid interface.

Momentum equation:

$$\rho_f\left(\frac{\partial \boldsymbol{u}}{\partial t}+(\boldsymbol{u}\cdot\nabla)\boldsymbol{u}\right)=-\nabla \boldsymbol{P}+\rho_f \boldsymbol{g}+\mu_f\nabla^2\boldsymbol{u} \tag{11}$$

$$\boldsymbol{P}=p+\rho_f \boldsymbol{g}\cdot\boldsymbol{x} \tag{12}$$

where $\boldsymbol{u}$ is the velocity of fluid; $\boldsymbol{P}$ is the total pressure; p is the fluid pressure; $\boldsymbol{g}$ is the acceleration due to gravity; and $\boldsymbol{x}$ is the vector. The first term is the fluid pressure, and the second term in the Eq. (12) represents the hydrostatic pressure. To obtain translational and rotational velocities of the sphere, Eqs. (10) and (11) were coupled with the equation of motion of sphere. Therefore, the equation of motion for the sphere in general 3D) cases is given by:

$$m\frac{d\boldsymbol{U}_p}{dt}=m\boldsymbol{g}+\int\left[-P\mathbf{1}+\tau\right]\cdot\boldsymbol{n}dS \tag{13}$$

$$\frac{d(\boldsymbol{I}\cdot\Omega_p)}{dt}=\int(\boldsymbol{x}-\boldsymbol{X}_p)\times\left(\left[-P\mathbf{1}+\tau\right]\cdot\boldsymbol{n}\right)dS \tag{14}$$

$$\boldsymbol{u}=\boldsymbol{U}_P+\Omega_p\times(\boldsymbol{x}-\boldsymbol{X}_p) \tag{15}$$

where m is the mass of the sphere; $\boldsymbol{U}_p$ is the translational particle velocity; Ω_p is the angular velocity; $\mathbf{1}$ is the unit tensor; $\boldsymbol{I}$ is the moment of inertia tensor; $\boldsymbol{x}$ is the vector (x-, y- and z-direction); and $\boldsymbol{X}_p$ is the coordinate of the centre of mass of the sphere. The mass of the sphere m and moment of inertia I were calculated by using the following expressions: $m=\rho_p\pi D_p^3/6$ and $I=\text{diag}(mD_p^2/10)$ [31,32].

3.2. Initial and boundary conditions

At the start of the simulation, both sphere and fluid were considered to be at rest in the duct. Hence, both fluid velocities as well as sphere velocities (linear and angular) in the duct were set to zero. No slip condition was used on the surface of the sphere and the duct wall. Table 1 provides the physical properties of the rigid sphere and the fluid that were incorporated in the simulations. In the next step, a transient simulation was initiated to track sphere movement. During each time step, the sphere and fluid velocities were updated with the help of Eqs. (10)–(15). The resultant updated information was used to represent the boundary conditions.

Table 1
Physical properties of particle and fluid used in simulations

Properties	Particle	Fluid (water)
Geometry	Sphere	–
Diameter, mm	1.62–4.0	–
Density, kg/m^3	1,297–1,916	998
Viscosity, kg/m s	–	9.5808×10^{-4}
Temperature, K	294	294
Density ratio	1.3–1.92	

3.3. Arbitrary Lagrangian–Eulerian (ALE) moving mesh technique

The sphere falling freely in a fluid at rest contained 6 degrees of freedom along each of the three directions (i.e., independent movement, translation and rotation that a sphere undergoes in the fluid). Consequently, the simulations under these conditions were computationally expensive and remained unanswered when they were carried out in smaller time steps. In this study, a methodology was developed by applying the ALE moving mesh technique to the commercial software ANSYS CFX® and adopting it in all simulations. Very fine and coarse meshes were generated to resolve the rapid changes that occurred in velocities and pressure near the sphere surface. The former mesh type (fine) was applied near the solid boundaries while the latter type (coarse) was made gradually away from the sphere surface.

With regard to the simulations in the present study, mesh quality was monitored based on the orthogonality angle of the moving mesh: if this parameter fell below 35°, then automatic re-meshing was carried out. The moving mesh ALE algorithm employed in this study was earlier presented by Suresh et al. [37]. This paper, however, presents the pictorial representation of the algorithm developed to carry out the ALE simulations (Fig. 2).

4. Solution methodology

The salient points of the solution methodology may be listed as follows:

- The commercially available software ANSYS CFX® V13 based on finite volume method was used to solve the governing Eqs. (10)–(12). The entire computational domain was defined in the global Cartesian coordinate frame. For discretisation of the advection term, CFX offers optional upwind high-resolution schemes with a special blend factor.
- For momentum equations, discretisation of the advection term was carried out by choosing the high-resolution scheme that uses a non-linear recipe with a blend factor, which is as close as possible to unity at each node and prevents non-physical undershoots and overshoots in the solution.
- Transient calculations were carried out using a robust and bounded second-order backward Euler scheme.
- The pressure correction scheme proposed by Rhie and Chie [38] based on co-locating pressure and velocity was used at the same grid points.
- The hydrodynamic equations for velocities and pressure were solved together as a single system by using ANSYS coupled solver.
- A multigrid technique was adopted to accelerate the convergence in solving linearised equations.
- For the solid sphere domain given by the equation of motion (Eq. (13)), ANSYS solver comprising two

algorithms was used as follows: (a) a linear momentum solver based on Newmark integration scheme (ANSYS CFX Documentation) [39] for the translation of sphere and (b) an angular momentum solver based on Simo-Wang algorithm for the rotation of the sphere [40].

A detailed description of the discretisation methodology of the governing equations along with its solutions (used in the present study) is discussed by Suresh et al. [37]. Other computational details of the solution methodology may be summed up; thus, the convergence criterion was fixed at residual root mean square (RMS) value of 10^{-4}; the time step for the transient simulations was the typically chosen 0.001 s such that the RMS courant number was <0.5, which is adequate to capture the sphere dynamics in the fluid at rest; similarly, the mesh numbers used in the simulations were typically about 1.77×10^5 nodes.

The simulations were carried out using Intel® Core i5-4570 CPU @ 3.2 GHz (4 GB RAM) on a Windows 7 platform. Twenty-four cases with different density ratios and particle Reynolds numbers were investigated. The spatial and temporal discretisation in the transient CFD simulations were time-consuming even with faster computers [41], and this observation holds good for all the cases studied in the present simulations. The transient simulations took substantial time, averaging 19 d to complete a single case study of a free-falling sphere in quiescent Newtonian fluid. Twenty-four cases with different sphere diameters and sphere-to-water density ratios (ρ_r) were studied; results of which are presented in this paper.

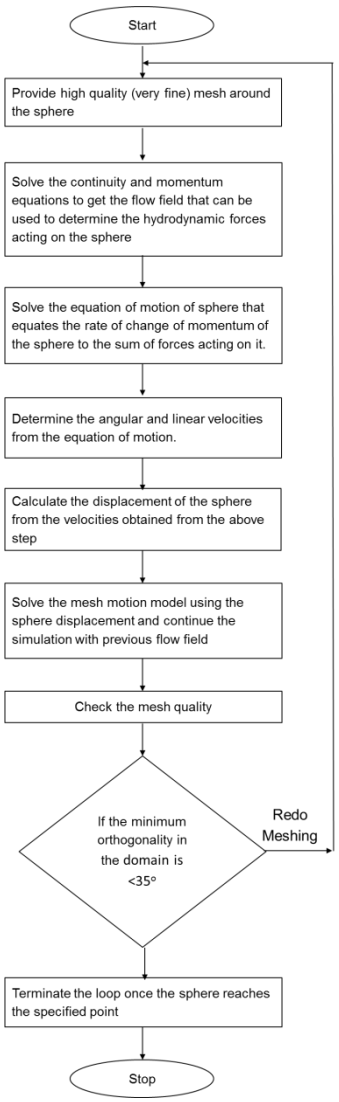

Fig. 2. Methodology developed to carry out ALE simulations for the unsteady behaviour of freely falling sphere in a Newtonian fluid at rest.

5. Results and discussion

5.1. Mesh independency test

Mesh independency test was performed for the entire computational domain with different mesh sizes as shown in Fig. 3. In the present investigation, the effect of different mesh sizes (coarse mesh = 177,870 nodes and fine mesh = 285,170 nodes) for one of the maximum density ratios (ρ_r = 1.9) was considered to study the mesh independency with a smaller time step of 8×10^{-3}. Fig. 3 displays the dimensionless displacement of spheres in *Y*-direction with respect to time obtained from the transient simulation results for density ratio 1.9 and sphere diameter 3 mm. The difference in the dimensionless displacement of two mesh sizes was <2%. Further mesh refining was not feasible owing to the limited features in computational resources. Therefore, the simulation studies in this undertaking used typical mesh sizes consisting of 1.77×10^5 nodes and found it adequate enough to evaluate the transient behaviour of sphere falling through the Newtonian fluid at rest.

5.2. Validation of results

Simulations were performed on spheres of varying diameters and density ratios (Table 1), with a blockage ratio of 0.01. A comparison of simulation results with the experimental results of Clift et al. [34] based on Best number (N_D) is

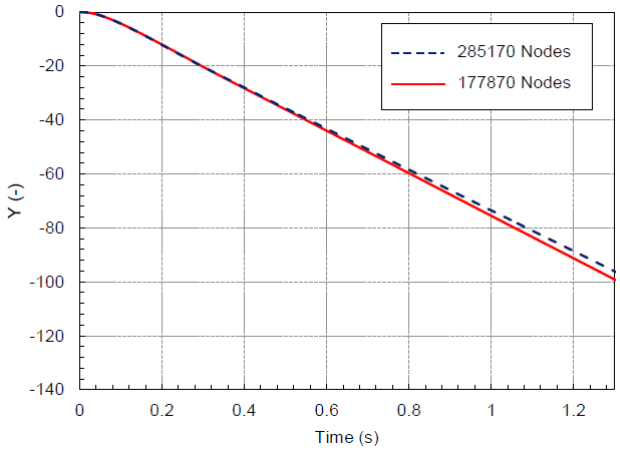

Fig. 3. Dimensionless displacement of sphere falling in *y*-direction with respect to time for two different mesh sizes (fine – 285,170 nodes and coarse – 177,870 nodes).

presented in Fig. 4. These findings reveal that the two sets of results are in good agreement for spheres with Re_p in the range of 572–803. A small difference between simulation and experimental results was evident for spheres with Re_p of 480, 644 and 1,091, which may be due to the increase in x-directional angular velocity of the spheres (Fig. 7(c)); it is also possible that there may be an increase in numerical error due to an increase in particle Reynolds numbers [24], which is not discussed in the present paper.

5.2.1. Terminal velocities of sphere

Velocity variation of sphere falling in quiescent water for the different particle diameters (1.62 mm < D_p < 4.0 mm) and the density ratios (1.72 < ρ_r < 1.92) is given in Fig. 5. It is seen from Fig. 5 that the time-averaged terminal velocity $\langle U_t \rangle$ of the sphere increases significantly with increase in particle diameter. For all the cases studied, it is noticed that the sphere with smaller diameter reaches the terminal velocity within shorter acceleration period, whereas the sphere with relatively large diameter reaches the terminal velocity slowly with longer acceleration period. Similar trend in velocity variation is also observed in analytical and analytical–numerical techniques developed by Jalaal et al. [17], Torabi et al. [18] and Nouri et al. [19]. Also from the point of physics, it is clear that increase in velocity of sphere decreases the drag coefficient (Fig. 6). Hence, the drag coefficient is strongly a function of velocity of sphere falling in a Newtonian fluid at rest.

Table 2 shows the time-averaged terminal settling velocity and corresponding Re_p of sphere in water for different diameters and density ratios studied. It is noticed from the Table 2 that the smaller diameter particle attained terminal settling velocity faster at corresponding low Re_p. For low Re_p < 210, the steady wake formed behind the sphere is

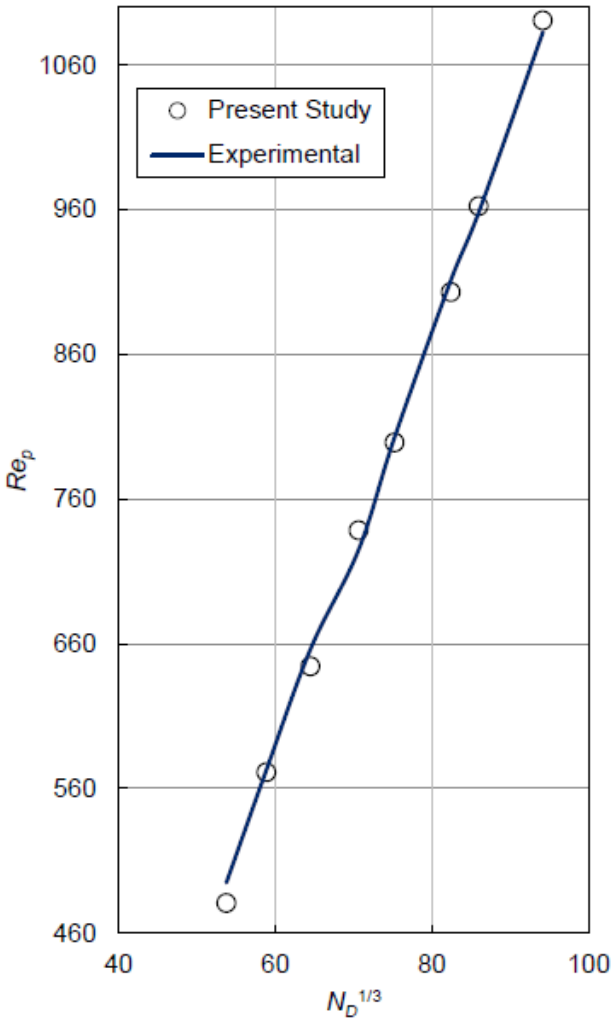

Fig. 4. Comparison of present study and the experimental results based on the particle Reynolds number (Clift et al. [34]).

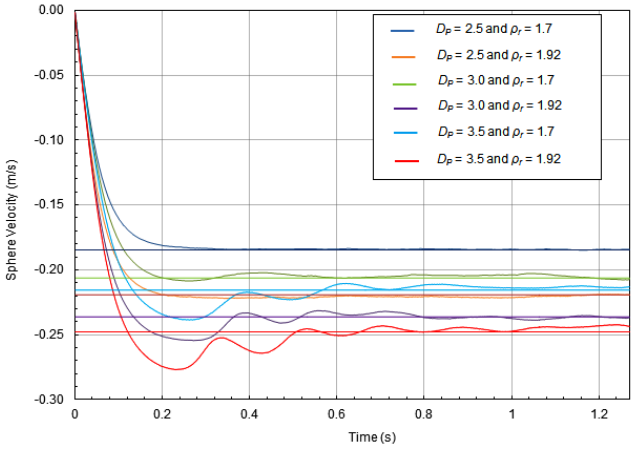

Fig. 5. Linear velocity of sphere falling in y-direction with respect to time for different particle diameters and density ratios. The solid coloured horizontal line represents the time-averaged terminal settling velocity of sphere. For the interpretation of colour lines in the above figure the reader is requested to refer the soft copy of this paper provided in web version.

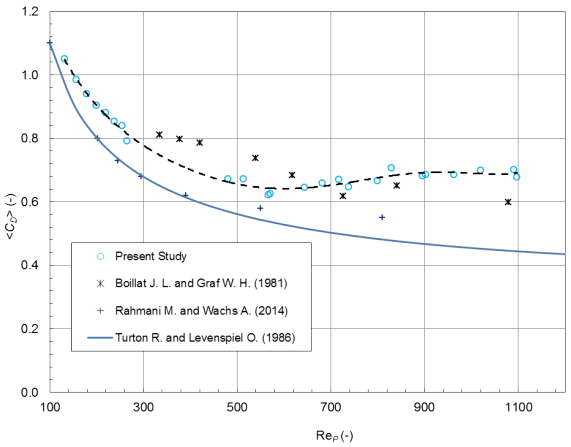

Fig. 6. Relationship between time-averaged drag coefficients and particle Reynolds number along with previously reported literature data. Dotted line represents the trend line for the present simulation data.

Table 2
Time-averaged terminal settling velocity $\langle U_t \rangle$ of sphere in water (ρ_f = 998 kg/m^3)

S. No.	D_p (m)	ρ_r	$\langle U_t \rangle$(m/s)	Re_p
1	0.00250	1.7	–0.18428	479.90
2	0.00250	1.92	–0.21930	571.09
3	0.00300	1.7	–0.20622	644.44
4	0.00300	1.92	–0.23629	738.41
5	0.00350	1.7	–0.21552	785.75
6	0.00350	1.92	–0.24770	903.07

axisymmetric as characterised by creeping flow and may not affect the terminal velocity significantly. On the other hand, as Re_p > 210 the instability in wake, angular velocities and non-vertical path may be ascribed to strong oscillations in terminal velocity. As a result increase in sphere diameter with higher density ratios leads to an increase in terminal velocity and its oscillations when sphere falling in a Newtonian fluid of constant density and viscosity [24,29,37].

5.2.2. Time-averaged drag coefficients

Fig. 5 presents the relationship between time-averaged drag coefficient $\langle C_D \rangle$ and particle Reynolds number Re_p. The time-averaged drag coefficients are obtained once the sphere reaches time-averaged terminal velocity. We compared $\langle C_D \rangle$ obtained from the present study with the empirical drag coefficient of Turton and Levenspiel [35] together with the outcomes of experimental and numerical drag coefficients from the published literature. The simulation results of $\langle C_D \rangle$ for density ratios between 1.3 and 1.92 with sphere diameter 1.62 mm were found to be below 8% when compared with the standard drag, and the corresponding Re_p was observed between 131 and 264. From Fig. 5, it is obvious that the $\langle C_D \rangle$ of a sphere falling in the Newtonian fluid agrees fairly well with the values of standard drag coefficient (solid drag curve) given by Eq. (6) until Re_p attains a value of 210 as reported by Rupesh et al. [29].

In this regime (131 < Re_p < 200), the wake formed behind the sphere may be attached, axisymmetric and may not affect the drag coefficient significantly. It is observed that the calculated percentage deviation between $\langle C_D \rangle$ and standard drag was increased with further rise in the particle Reynolds number (Re_p > 200). For the Re_p between 450 and 1,091, density ratios of 1.7–1.92 and sphere diameters between 2.5 and 4.0 mm, the $\langle C_D \rangle$ obtained from the simulation is relatively higher when compared with experimental results of Boillat and Graf [21] and numerical results of Rahmani and Wachs [42]. The $\langle C_D \rangle$ values obtained under the Re_p regime from 219 to 1,091 in this present study show a reasonable corroboration with <10% deviation. This may be attributed to increase in non-axisymmetric wake, rotation of sphere and deviation of sphere trajectory from vertical to non-vertical [20]. Also to confirm the qualitative agreement of the present study with literature values of $\langle C_D \rangle$ for Re_p > 210, we performed simulation for one case with density ratio of 2.5 (heavier falling sphere), and the results obtained are shown in Table 3.

Table 3
Validation of present simulation $\langle C_D \rangle$ with literature values

Literature	ρ_r	Re_p	$\langle C_D \rangle$
Rahmani and Wachs [42]	2.56	295	0.650
Horowitz and Willamson [14]	2.54	360	0.681
Present study	2.50	361	0.696
Present study	1.92	264	0.791

It is clear from Table 3 that the present study well agrees with the standard drag coefficient (Fig. 6) for heavier particles (ρ_r = 2.50 and 1.92). However, the range of relative density difference between the particle and fluid in this study was considered as lower when compared with literature values (Rahmani and Wachs [42], and Horowitz and Willamson [14]). Therefore, the rotation of falling spheres in Newtonian fluid at rest, which is shown in Fig. 7, and non-vertical trajectories along the moving direction (i.e., as sphere descends from the initial position), which are exhibited in Figs. 8 and 9, may be attributed to the higher deviation in $\langle C_D \rangle$, and small disturbance of fluid wake structure on sphere may lead to deviate the sphere from the vertical path for lighter falling sphere with an enhanced drag coefficient.

5.2.3. Trajectories of sphere

Figs. 8 and 9 give the trajectories (path taken by the spheres) of spheres falling freely through a Newtonian fluid (water) at rest under gravity in *XY*-direction with respect to time for the sphere diameters 1.62–4.00 mm, and density ratios of 1.7 and 1.92. A standard travelling distance of 0.4 m from the sphere's initial position in the duct was considered for all the cases presented here, in order to obtain reliable and accurate information. For ρ_r = 1.7 at particle Reynolds number 219, the sphere followed almost an oblique and steady path a little distance away from the centre of the duct as shown in Fig. 8. No significant oscillations were found at this stage in comparison with other particle Reynolds numbers. To explain further, at ρ_r =1.7 and Re_p = 219, the wake generated behind the sphere is axisymmetric and attached behind the sphere as it falls at initial transient of say 0.2 s. As the time interval progresses, the wake behind the sphere breaks up, i.e., loses its axisymmetric structure and induces rotational movement of the sphere with a small angular velocity, thereby resulting in a small deviation of path from the duct's centre of axis. With a further increase in Re_p to 481 at ρ_r = 1.7, the sphere followed non-periodic oscillations in its vertical path around the centre of axis of the duct.

The sphere trajectories were found to be oblique with oscillations for Re_p 799 and 963. On the other hand, at ρ_r =1.92 and Re_p = 265, spheres showed non-periodic oscillations in the vertical direction. At this stage, the observed rotation of spheres was relatively higher when compared with Re_p = 265 at ρ_r =1.7 due to the breakup of axisymmetric wake behind the sphere. Further increase in particle Reynolds number (571) at ρ_r = 1.92, up to a time period of 0.15 s resulted in the sphere following a vertical path with a sudden noticeable deviation from the vertical direction after 0.15 s and a subsequent return back toward the axis of the duct accompanied by oscillations around the axis. At Re_p = 738 and 903, the spheres showed a steady and unsteady oblique path, respectively; whereas for

Re_p = 1,091, the sphere followed an oblique path with periodic oscillations. It is also noticed in Fig. 9 that if we block the sphere rotation numerically, the trajectory deviation from the centerline reduces. Similar results on trajectory shift from the centerline are also reported by Jenny et al. [13] and Horowitz and Williamson [14]. All the trajectories obtained from simulation results of the present study (shown in Figs. 8 and 9) agreed favourably with published experimental and numerical data [14,42]. It has also come to light that the trajectory path of spheres is determined by the important role played by criteria like wake formation, growth and detachment of counter rotating vortex behind the sphere, and the rotation of sphere due to wake transition scenario [29].

5.2.4. Effect of angular velocity of sphere on transient drag coefficient

From the simulation results, it is observed that the angular velocity of sphere in *x*-direction is significant when compared with *y*- and *z*-direction (Figs. 7(a) and (b)). Therefore, *x*-directional angular velocity is considered for analysis and discussion. Fig. 7(c) demonstrates that angular velocity of the sphere in *x*-direction increases with a rise in particle Reynolds number. It is evident that when the particle Reynolds number falls below 210, the magnitude of angular velocity is relatively lower because the wake behind the falling sphere may not have a significant effect on its angular velocity. As the particle Reynolds number rises above 260, wake behind the falling sphere loses axisymmetric; in turn, wake shedding induces the particle to rotate, and consequently, the sphere migrates away from the centre, taking up instead a steady oblique as well as unsteady oblique path (Figs. 8 and 9).

Furthermore, when the particle Reynolds number becomes <260, the angular velocity is low, and the drag coefficient at this regime is found to be minimum in comparison with standard drag (Fig. 6). On the other hand, when particle Reynolds numbers exceed 260, the angular velocity of the sphere increases, and as a result, the drag coefficient also goes up in comparison with the standard drag. It therefore follows that the drag coefficient of spheres may be enhanced with an increase in angular velocity in the moving direction of the sphere relative to the fluid at rest.

Figs. 10(a) and (b) show a comparison between the simultaneous variation of drag coefficient and *x*-directional

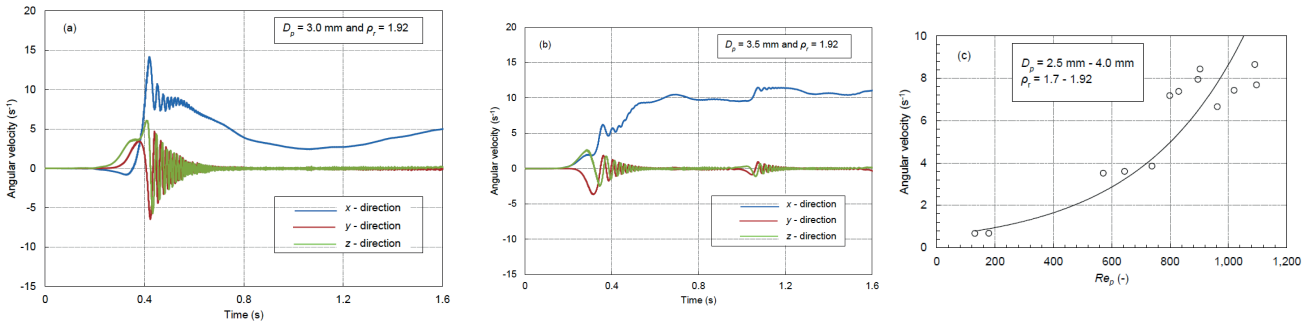

Fig. 7. (a) and (b) angular velocity of sphere vs. time in *x*-, *y*- and *z*-direction and (c) time-averaged angular velocity (*x*-directional) vs. particle Reynolds number.

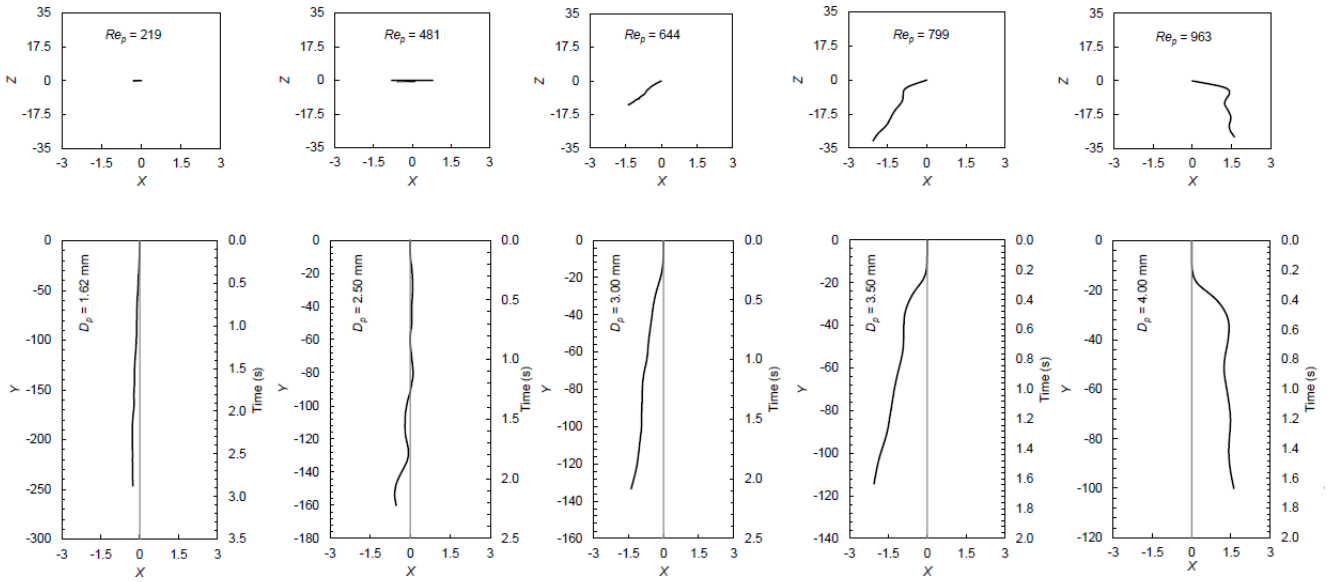

Fig. 8. 2-Dimensional trajectories of sphere falling in a quiescent water at ρ_r = 1.7 for five different sphere diameters (1.62, 2.5, 3.0, 3.5 and 4 mm) and their corresponding particle Reynolds numbers (219, 481, 644, 799 and 963). The top row from left to right represents the top view of sphere path and the bottom row represents the front view of 2-Dimensional trajectories.

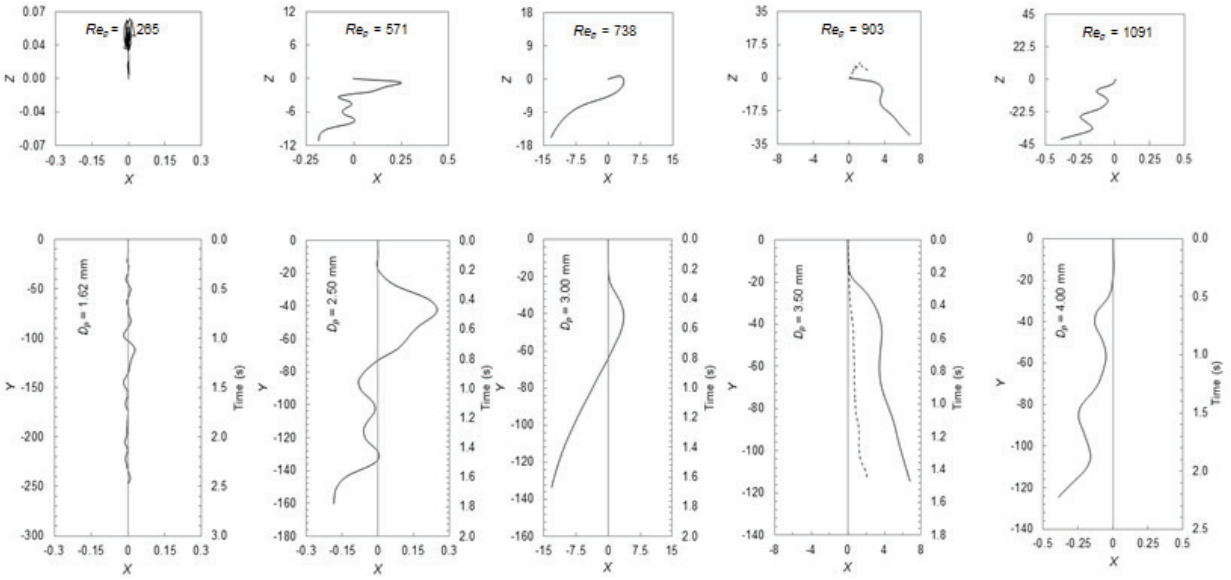

Fig. 9. 2-Dimensional trajectories of sphere falling in a quiescent water at ρ_r = 1.92 for five different sphere diameters (1.62, 2.5, 3.0, 3.5 and 4 mm) and corresponding particle Reynolds numbers (265, 571, 738, 903 and 1,091). The dotted path in the particle Reynolds number 903 is by blocking the numerical rotation. The top row from left to right represents the top view, and the bottom row represents the front view of 2-Dimensional trajectories.

angular velocity between the fixed sphere and falling sphere in a Newtonian fluid at rest. The standard drag for the fixed sphere with respect to time is constant and steady, whereas the drag coefficient for a sphere freely falling in a fluid at rest decreases at initial time periods, oscillates and gradually stabilises with progress of the time interval. Similar patterns of oscillation are also exhibited in the linear velocity of spheres of diameters 3.0 and 3.5 mm (Fig. 5). The terminal velocity was obtained once the acceleration of the sphere reached zero from the initial position as given in Fig. 5.

Mordant and Pinton [22] also reported similar oscillatory trends with respect to time. The angular velocity of the sphere on the other hand is not seen until a time period of 0.14 s, at which point the drag coefficient decreases for spheres with diameter 3.0 and 3.5 mm; as soon as the sphere crosses a time period of 0.2 s, there is a significant level of rotation experienced by spheres of the mentioned diameters, followed by an increase in drag coefficient (Figs. 10(a)–(b)). With progress in time, there is clear evidence of an increase in rotation of the falling sphere accompanied by a decrease in drag coefficient (Figs. 10(a) and (b)). The transient drag coefficient for actual case (without blocking numerical rotation) and numerically blocked rotation are plotted as shown in Fig. 10(a). If the rotation is blocked numerically, the drag coefficient is lesser than the actual case (ρ_r = 1.92 and D_p = 3.0 and 3.5 mm) where both the non-vertical trajectory and rotation were happened in the falling sphere (Fig. 9). However, the drag coefficient of numerically blocked rotation case has higher than the standard drag coefficient as shown in horizontal dotted lines of Figs. 10(a) and (b). This is due to non-vertical trajectory, which was reflected to rise in the transient drag coefficient.

Based on the above findings, it may be inferred that the drag coefficients of falling spheres depart from the standard drag due to a significant level of rotation experienced by a sphere falling in Newtonian fluid at rest. The angular velocity of the sphere may be a possible reason for enhancement of the drag coefficient as confirmed by published experimental data [21].

5.2.5. Lift coefficient of freely falling spheres

The transient lift coefficient of spheres falling freely in a Newtonian fluid at rest was calculated using the relation as given in Eqs. (8) and (9). The values thus obtained were plotted with respect to time (Figs. 11 and 12). From the figures, it is clear that the onset of lift coefficient commenced at the initial transient (0.14 s) for all sphere diameters studied with density ratios 1.7–1.92. The immediate detachment of axisymmetric vortex behind the sphere induced a rotational movement in the sphere, and a resultant lift force was generated. Fig. 12 shows the magnitude of lift coefficient at ρ_r = 1.7 and Re_p = 799 with a negative sign (–ve), whereas at ρ_r = 1.7 and Re_p = 963 the same parameter has a positive sign (+ve). In contrast, at ρ_r = 1.92 for Re_p 738 and 903, a positive sign is evident in the magnitude of lift coefficient. These +ve and –ve signs denote the orientation of the *XY* plane of symmetry that governs the trajectory of the sphere as already reported [29]. Similar behaviour was observed in the simulations performed in the present study (Figs. 8 and 9). For instance, the sphere trajectories as seen in Figs. 8 and 9 indicate that a lift force is experienced by the sphere in the direction of movement when the sphere falls from its original position. Additionally, it confirms that the lift coefficient is responsible for the sphere to change its orientation from vertical fall.

5.2.6. Sphere residence time

Fig. 13 gives the residence time, i.e., the time taken by the sphere to cross a standard distance of 0.4 m in the Newtonian fluid at rest contained in a square duct. The method used

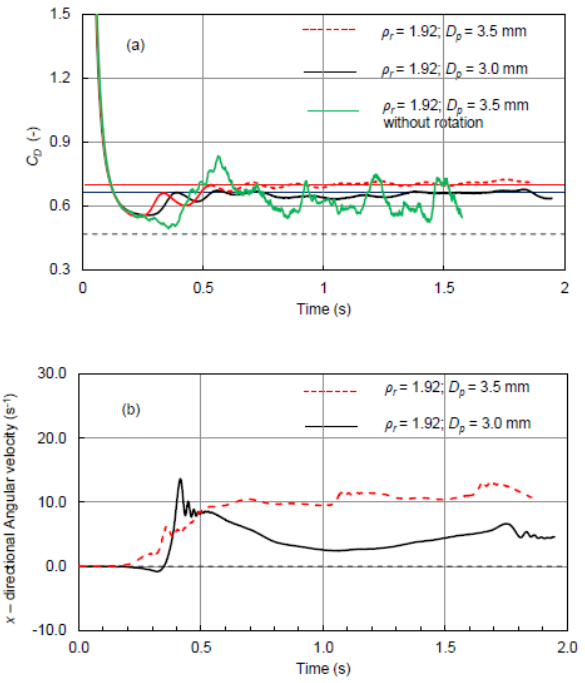

Fig. 10. Simultaneous variation of drag coefficient: (a) drag coefficient with time and (b) angular velocity (x-direction) with time for two different particles (3.0 and 3.5 mm) at ρ_r = 1.92.
Note: In (a) and (b) horizontal dotted line represents the standard drag and angular velocity of fixed sphere with time. In (a), solid horizontal line indicates the average drag coefficient spheres. Green coloured solid line shows the result obtained for the simultaneous variation of drag coefficient of sphere at ρ_r = 1.92 and D_p = 3.5 mm through numerically blocked rotation of sphere.

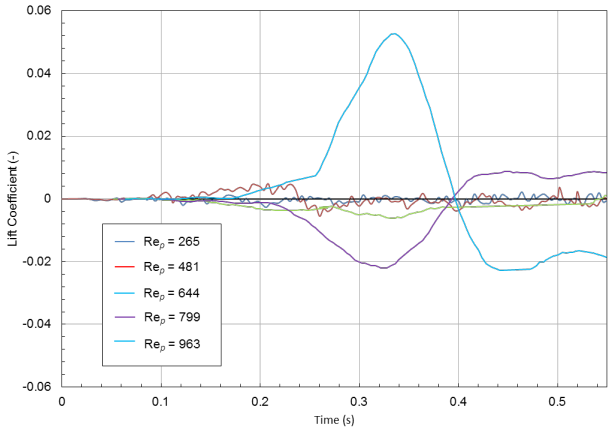

Fig. 11. Lift coefficient of sphere falling in quiescent water with respect to time at density ratio of 1.7.

for the determination of residence time is discussed elsewhere [36,43]. In Fig. 13, density ratios of 1.7 and 1.92 for sphere diameters from 1.62 to 4 mm were considered. The observations unravel the fact that at lower density ratios, the residence time of spheres was found to be longer, whereas at higher density ratios, it was relatively shorter. It may

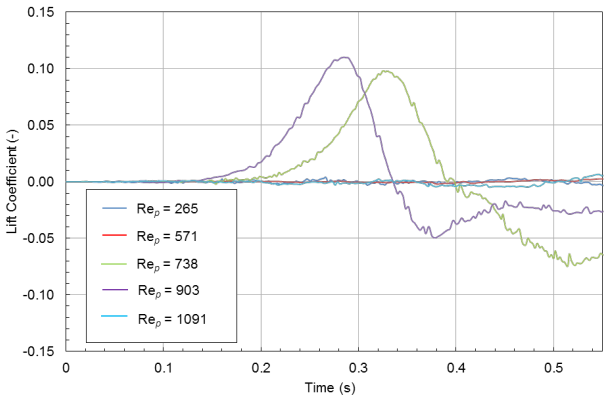

Fig. 12. Lift coefficient of sphere falling in quiescent water with respect to time at density ratio of 1.92.

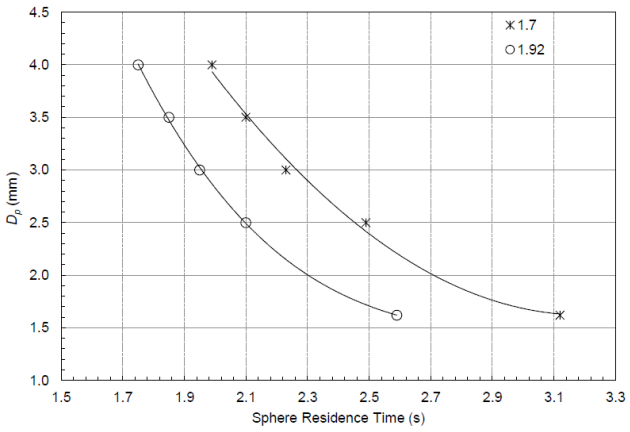

Fig. 13. Sphere size vs. the sphere residence time the solid line represents the trend of sphere diameters with respect to time for two density ratios (1.7 and 1.92).

therefore be interpreted that the lower the density ratio, longer the residence time, and similarly, the higher the density ratio, the shorter the residence time.

6. Conclusion

In the present investigation, ALE simulation was successfully employed using ANSYS CFX®V13 software to understand the intricacies of the unsteady behaviour demonstrated by spheres falling in Newtonian fluid at rest for a range of intermediate Reynolds numbers (131–1,097). The results obtained from the ALE simulations were validated with the experimental and numerical data that are already available in research literature. The key conclusion from the present study is summarised as follows:

- The transient simulations performed in this study consumed significant amounts of time across all the density ratios and particle diameters that were investigated: 19 d were required for each of the 24 cases being examined.
- The drag coefficient of a sphere falling in Newtonian fluid agreed reasonably well with standard drag up to a particle Reynolds number of 210, after which it deviated from

the standard drag with a rise in particle Reynolds number above 210. The observed deviation can be attributed to the influence of angular velocity of the sphere.
- It was also observed that the onset of angular velocity of sphere and generation of lift force deviated the orientation of the sphere from the centre of axis of the duct as a result of which the sphere adopted a variety of trajectories such as vertical steady oblique, vertical oscillatory, unsteady oblique or oblique oscillatory path along the moving direction.
- The magnitude of lift coefficient in +ve and –ve signs indicated the orientation of the *XY* plane of symmetry in sphere trajectory.
- It may be stated here that the ANSYS CFX® V13 software was found to be sufficient to capture the unsteady behaviour of sphere falling in a Newtonian fluid at rest.
- However, for higher particle Reynolds (i.e., those with Re_p > 1,000), very fine meshes, smaller time steps in high-speed supercomputing and the selection of suitable turbulence models are crucial to capture accurate sphere dynamics and wake-sphere interactions.

Therefore, the methodology used to carry out ALE simulations in this direction can be refined further and applied for the examination of different particle geometries. It can also be extended to comprehend the trends followed by multiparticle systems in two-phase flows.

Acknowledgements

We would like to thank Dr. Prabhakar, Dr. AshishKapoor, Dr. Sasidharan for their invaluable discussions. We would also like to thank Dr. Rajesh and the management of SRM University for permission to use computational facilities.

Symbols

C_D	—	Local drag coefficient
$\langle C_D \rangle$	—	Time-averaged drag coefficient
C_L	—	Lift coefficient
$\langle C_L \rangle$	—	Time-averaged lift coefficient
C_p	—	Dimensionless surface pressure of sphere
D_p	—	Diameter of the sphere, m
D_t	—	Width or breath of the duct, m
D_x	—	Displacement of sphere in *x*-direction
D_y	—	Displacement of sphere in *y*-direction
D_z	—	Displacement of sphere in *z*-direction
f	—	Darcy friction factor
$\boldsymbol{g}$	—	Acceleration due to gravity, m/s^2
m	—	Mass of the sphere, kg
$\boldsymbol{P}$	—	Total pressure, N/m^2
p	—	Fluid pressure, N/m^2
P_s	—	Sphere surface pressure, N/m^2
Re_p	—	Particle Reynolds number
U_t	—	Terminal velocity of sphere, m/s
$\langle U_t \rangle$	—	Time-averaged terminal velocity of sphere, m/s
$\boldsymbol{U}_p$	—	Translational velocity, m/s
u	—	Velocity, m/s
V_s	—	Front stagnation velocity, m/s
$\boldsymbol{x}$	—	Vector (*x*-, *y*- and *z*-direction)
X	—	Dimensionless displacement of sphere in *x*-direction
Y	—	Dimensionless displacement of sphere in *y*-direction
Z	—	Dimensionless displacement of sphere in *z*-direction

Greek

∇	—	Del operator
μ_f	—	Viscosity of water, kg/m·s
ρ_f	—	Density of water, kg/m^3
ρ_p	—	Density of sphere, kg/m^3
τ_{ij}	—	Shear stress, N/m^2
Ω	—	Angular velocity, rad/s

References

[1] C.E. Lapple, C.B. Shepherd, Calculation of particle trajectories, Ind. Eng. Chem., 32 (1940) 605–617.
[2] J.F. Richardson, W.N. Zaki, Sedimentation and fluidization: Part 1, Trans. Inst. Chem. Eng., 32 (1954) S82–S100.
[3] E.B. Christiansen, D.H. Barker, The effect of shape and density on free settling of particles at high Reynolds numbers, AIChE J., 11 (1965) 145–151.
[4] G.E. Stringham, D.B. Simons, H.P. Guy, The Behavior of Large Particles Falling in Quiescent Liquids, US Geological Survey Professional Paper 562 C, 1969, pp. C1–C36.
[5] R. Elgaddafi, R. Ahmed, M. George, F. Growcock, Settling behavior of spherical particles in fiber-containing drilling fluids, J. Pet. Sci. Eng., 84–85 (2012) 20–28.
[6] R. Elgaddafi, R. Ahmed, F. Growcock, Settling behavior of particles in fiber containing Herschel Bulkley fluids, Powder Technol., 301 (2016) 782–793.
[7] S.N. Shah, Proppant settling correlations for non-Newtonian fluids under static and dynamic conditions. Soc. Petrol. Eng. J., 22 (1982) 164–170.
[8] S.N. Shah, Y. El Fadili, R.P. Chhabra, New model for single spherical particle settling velocity in power law (visco-inelastic) fluids, Int. J. Multiphase Flow, 33 (2007) 51–66.
[9] R. Kuriakose, C. Anandharamakrishnan, Computational fluid dynamics (CFD) applications in spray drying of food products, Trends Food Sci. Technol., 21 (2010) 383–398.
[10] I. Newton, The Principia: Mathematical Principles of Natural Philosophy, University of California Press, Berkley, 1999.
[11] G. Stokes, On the effect of internal friction of fluids on the motion of pendulums, Trans. Cambridge Philos. Soc., 9 (1851) 8.
[12] G. Kuwabara, S. Chiba, K. Kono, Anomalous motion of a sphere falling through water, J. Phys. Soc. Jpn., 52 (1983) 3373–3381.
[13] M. Jenny, G. Bouchet, J. Dušek, Nonvertical ascension or fall of a free sphere in a Newtonian fluid, Phys. Fluids, 15 (2003) L9–L12.
[14] M. Horowitz, C.H.K. Willamson, The effect of Reynolds number on the dynamics and wakes of freely rising and falling spheres, J. Fluid Mech., 651 (2010) 251–294.
[15] P. Ern, F. Risso, D. Fabre, J. Magnaudet, Wake-induced oscillatory paths of bodies freely rising or falling in fluids, Annu. Rev. Fluid Mech., 44 (2012) 97–121.
[16] M. Hartman, J.G. Yates, Free-fall of solid particles through fluids, Collect. Czech. Chem. Commun., 58 (1993) 961–982.
[17] M. Jalaal, D.D. Ganji, G. Ahmadi, Analytical investigation on acceleration motion of a vertically falling spherical particle in incompressible Newtonian media, Adv. Powder Technol., 21 (2010) 398–304.
[18] M. Torabi, H. Yaghoobi, Novel solution for acceleration motion of a vertically falling spherical particle by HPM-padé approximant, Adv. Powder Technol., 22 (2011) 674–677.
[19] R. Nouri, D.D. Ganji, M. Hatami, Unsteady sedimentation analysis of spherical particles in Newtonian fluid media using analytical methods, Propul. Power Res., 3 (2014) 96–105.

[20] D. Karamanev, L. Nikolov, Free rising spheres do not obey Newton's law for free settling, AIChE J., 38 (1992) 1843–1846.
[21] J.L. Boillat, W.H. Graf, Settling velocity of spherical particles in calm water, J. Hydraul. Div., 107 (1981) 1123–1796.
[22] N. Mordant, J.F. Pinton, Velocity measurement of a settling sphere, Eur. Phys. J. B, 18 (2000) 343–352.
[23] H. Niazmand, M. Renksizbulut, Surface effect on transient three-dimensional flows around rotating sphere at moderate Reynolds numbers, Comput. Fluids, 32 (2003) 1405–1433.
[24] Z. Yu, N. Phan-Thien, R.I. Tanner, Dynamic simulation of sphere motion in a vertical tube, J. Fluid Mech., 518 (2004) 61–93.
[25] M. Horowitz, C.H.K. Willamson, Critical mass and a new periodic four-ring vortex wake mode for freely rising and falling particle, Phys. Fluids, 20 (2008) 101701.
[26] M. Jenny, G. Bouchet, J. Dušek, Instabilities and transition of a sphere falling or ascending freely in a Newtonian fluid, J. Fluid Mech., 508 (2004) 201–239.
[27] C.H.J. Veldhuis, A. Biesheuvel, An experimental study of regimes of motion of spheres falling or ascending freely in a Newtonian fluid, Int. J. Multiphase Flow, 33 (2007) 1074–1087.
[28] C.H.J. Veldhuis, A. Biesheuvel, D. Lohse, Freely rising solid spheres, Int. J. Multiphase Flow, 35 (2009) 312–322.
[29] K.R. Rupesh, J.B. Joshi, K. Nandakumar, P. Minev, Direct numerical simulations of a freely falling sphere using fictitious domain method: breaking of axisymmetric wake, Chem. Eng. Sci., 65 (2010) 2159–2171.
[30] W. Zhou, J. Dušek, Chaotic states and order in the chaos of the paths of freely falling and ascending spheres, Int. J. Multiphase Flow, 75 (2015) 205–223.
[31] H.H. Hu, N.A. Patankar, M.Y. Zhu, Direct numerical simulations of fluid–solid systems using the arbitrary Lagrangian–Eulerian technique, J. Comput. Phys., 169 (2001) 427–462.
[32] B.H. Yang, J. Wang, D.D. Joseph, H.H. Hu, T.-W. Pan, R. Glowinski, Migration of sphere in tube flow, J. Fluid Mech., 540 (2005) 109–131.
[33] N. Al Quddus, A.M. Walied, S. Bhattacharjee, Motion of a spherical particle in a cylindrical channel using arbitrary Lagrangian–Eulerian method, J. Colloid Interface Sci., 317 (2008) 620–630.
[34] R. Clift, J.R. Grace, M.E. Weber, Bubbles, Drops and Particles, Academic Press, Dover Publications, New York, 1978.
[35] R. Turton, O. Levenspiel, A short note on the drag correlation for spheres, Powder Technol., 47 (1986) 83–86.
[36] K. Suresh, A. Kannan, Effects of particle diameter and position on the hydrodynamics around a confined sphere, Ind. Eng. Chem. Res., 50 (2011) 13137–13160.
[37] K. Suresh, S. Balasubramanian, R. Karthikeyan, Transient drag coefficients from a freely rising and falling solid sphere at moderate particle Reynolds number, Can. J. Chem. Eng., 94 (2016) 1003–1014.
[38] C.M. Rhie, W.L. Chie, Numerical study of the turbulent flow past an airfoil with trailing edge separation, AIAA J., 21 (1983) 1525–1532.
[39] ANSYS CFX Documentation, ANSYS Inc., Canonsburg, PA, 2000.
[40] J.C. Simo, K.K. Wong, Unconditionally stable algorithms for rigid body dynamics that exactly preserve energy and momentum, Int. J. Numer. Methods Eng., 31 (1991) 19–52.
[41] K. Neeharika, A. Kannan, M.U.S.V. Aditya Varadhan, Quantifying enhancement in heat transfer due to natural convection during canned food thermal sterilization in a still retort, Food Bioprocess Technol., 4 (2011) 429–450.
[42] M. Rahmani, A. Wachs, Free falling and rising of spherical and angular particles, Phys. Fluids, 26 (2014) 083301-24.
[43] N.S. Cheng, Comparison of formulas for drag coefficient and settling velocity of spherical particles, Powder Technol., 189 (2009) 395–398.